Mon. Not. R. Astron. Soc. **000**, 000–000 (0000) Printed 1 February 2008 (MN LATEX style file v1.4)

Comparing the SFI Peculiar Velocities with the PSCz Gravity Field: a VELMOD analysis

E. Branchini[1,2], W. Freudling[3,4], L.N. Da Costa[4], C.S. Frenk[5]
R. Giovanelli[6], M.P. Haynes[6], J.J. Salzer[7], G. Wegner[8], I. Zehavi[9]

[1] *Kapteyn Institute, University of Groningen, Landleven 12, P.O. Box 800, 9700, Groningen, The Netherlands.*
[2] *Dipartimento di Fisica dell'Universitá degli Studi "Roma TRE", Via della Vasca Navale 84, I-00146, Roma, Italy.*
[3] *Space Telescope – European Coordination Facility, Karl-Schwarschild Strasse 2, 85748, Garching, Germany.*
[4] *European Southern Observatory, Karl-Schwarschild Strasse 2, 85748, Garching, Germany.*
[5] *Department of Physics, University of Durham, South Rd., DH1 3LE, Durham, U.K.*
[6] *Center for Radiophysics and Space Research and National Astronomy and Ionosphere Center. Cornell University, Ithaca, NY 14853, USA.*
[7] *Astronomy Department, Wesleyan University, Middletown, CT 06457, USA.*
[8] *Department of Physics and Astronomy, Darmouth College, Hanover, NH 03755, USA.*
[9] *NASA/Fermilab Astrophysiscs Group, Fermi National Accelerator Laboratory, Batavia, IL 60510-0500, USA.*

1 February 2008

ABSTRACT

We compare the peculiar velocities derived from the I-band Tully-Fisher (TF) relation for 989 field spiral galaxies in the SFI catalogue with the predicted velocity field derived from the IRAS PSCz galaxy redshift survey. We assume linear gravitational instability theory and apply the maximum likelihood technique, VELMOD (Willick *et al.* 1997b), to SFI galaxies within cz$<$ 6000 km s^{-1}. The resulting calibration of the TF relation is consistent with a previous, independent calibration for a similar sample of spirals residing in clusters. Our analysis provides an accurate estimate of the quantity $\beta_I \equiv \Omega_m^{0.6}/b_I$, where b_I is the linear biasing parameter for IRAS galaxies. Using the forward TF relation and smoothing the predicted velocity field with a Gaussian filter of radius 300 km s^{-1}, we obtain $\beta_I = 0.42 \pm 0.04$ (1-σ uncertainty). This value, as well as other parameters in the fit, are robust to varying the smoothing radius to 500 km s^{-1} and splitting the sample into spherical shells in redshift space. The one exception is the small-scale velocity dispersion, σ_v, which varies from ~ 200 km s^{-1} within cz$_{LG} = 4000$ km s^{-1} to ~ 500 km s^{-1} at larger distance. For $\beta_I \simeq 0.42$, the residuals between the TF data and the PSCz gravity field are uncorrelated, indicating that the model provides a good fit to the data. More generally, a χ^2 statistic indicates that the PSCz model velocity field provides an acceptable (3σ) fit to the data for $0.3 < \beta_I < 0.5$.

Key words: Cosmology: theory — galaxies: clustering — large-scale structure — large–scale dynamics — cosmology: observations — galaxies: distances and redshifts

1 INTRODUCTION

Measurements of peculiar motions provide a fundamental tool to probe the mass distribution in the local universe. In the linear regime of gravitational instability, a simple relation between peculiar velocity, $\mathbf{v}$, and mass density contrast, δ_m, can be easily obtained from mass conservation, either in differential

$$\nabla \cdot \mathbf{v} = -\Omega_m^{0.6} \delta_m, \tag{1}$$

or integral form,

$$\mathbf{v}(\mathbf{r}) = \frac{\Omega_m^{0.6}}{4\pi} \int d^3\mathbf{r\prime} \frac{\delta_m(\mathbf{r\prime})(\mathbf{r\prime} - \mathbf{r})}{|\mathbf{r\prime} - \mathbf{r}|^3}, \tag{2}$$

where Ω_m is the cosmological mass density parameter. Together with the commonly used simplifying assumption of linear biasing, $\delta_g = b_g \delta_m$, where δ_g is the galaxy density contrast and b_g the galaxy biasing parameter, these two equations provide a relation between observable quantities: the peculiar velocity of luminous objects, $\mathbf{v}$, and the density contrast, δ_g, which can be obtained from large all-sky redshift surveys. The IRAS Point Source Catalogue (Beichman *et al.* 1998) is particularly suited for this purpose because of the good sky coverage and homogeneity of the survey. In this paper, we present a comparison of peculiar velocity data with a redshift survey based on the IRAS catalogue. Throughout the paper, we will use the subscript $_I$ to indicate that an IRAS density field has been used.

Comparing δ_g with $\mathbf{v}$ using any of the two equations above allows us to estimate the quantity $\beta_g = \Omega_m^{0.6}/b_g$ and to test the validity of the gravitational instability hypothesis. Although the two equations (1) and (2) are mathematically equivalent, they lead to two different strategies for measuring β_g. Equation 1 is used to perform the so-called density-density (d-d) comparisons which typically consist of the following steps: a 3-D velocity field reconstruction from observed radial velocities; differentiation of $\mathbf{v}(\mathbf{r})$ and use of eqn. (1) to compute δ_g; comparison to the observed galaxy density fields. The first step is the least trivial and requires some additional theoretical assumptions. Bertschinger & Dekel (1989) successfully implemented a d-d technique by assuming that $\mathbf{v}(\mathbf{r})$ is irrotational, in the POTENT reconstruction method. The many applications of POTENT to various datasets have consistently led to large values of β_I consistent with unity (see Sigad *et al.* 1998 and references therein). Equation (2) is at the core of the so-called velocity velocity (v-v) comparisons. In this approach, one computes the mass density field obtained from the galaxy distribution in the redshift survey, uses equation (2) to predict a peculiar velocity field and then compares it with the observed galaxy velocities. The v-v methods have been applied to most of the catalogues presently available and have given values of β_I which are typically in the range $0.4 - 0.6$ (see Willick 2000, for an updated summary of the various results).

The v-v methods are commonly regarded as more reliable and robust than the d-d ones because they require less manipulation of the data. The values of β_I obtained by these analyses are significantly smaller than unity, irrespective of the velocity tracers, model gravity field and comparison technique used. However, some of the v-v analyses showed evidence for a poor match between models and data, which would render the estimate of β_I meaningless. Davis, Nusser & Willick (1996) used their ITF technique (Nusser & Davis 1994) to compare the gravity field derived from the IRAS 1.2 Jy survey (Fisher *et al.* 1995) with the peculiar velocities obtained from the Mark III catalogue (Willick *et al.* 1995, 1996, 1997a). The coherent dipole residuals that they found were taken as evidence for significant discrepancies between modeled and observed velocity fields. Willick *et al.* (1997b, V1 hereafter) and Willick & Strauss (1998, V2 hereafter) also considered the IRAS 1.2 Jy velocity predictions and the Mark III dataset but compared them using the VELMOD method. They were able to obtain a good fit to the data only by introducing a physically motivated, external quadrupole contribution to the model velocity field. Da Costa *et al.* 1998 (D98 hereafter) found good agreement between the peculiar velocities of galaxies in the SFI catalogue (Haynes *et al.* 1999a, 1999b) and those derived from the IRAS 1.2Jy gravity field, by performing an ITF comparison. The same ITF method has been recently applied to compare two different datasets: the IRAS PSCz redshift survey (Saunders *et al.* 2000) and the peculiar velocities in the recently completed ENEAR catalogue (da Costa *et al.* 2000). Also in this case the agreement between model and data was satisfactory (Nusser *et al.* 2000).

In this paper, we use the VELMOD technique to compare the PSCz velocity prediction to the SFI dataset. As for any v-v comparison our main aim is to constrain β_I and to investigate the adequacy of the PSCz model velocity field. However, rather than simply adding one more measurement of β_I to those already in the literature from other v-v comparisons, we hope to address some more specific questions which should help simplify the rather complicated picture that has emerged from the results of the various v-v comparisons. Our goal is to check whether the PSCz–IRAS gravity field still provides a good fit to SFI data when the comparison is performed with the VELMOD method rather than the ITF. We also want to exploit fully the denser and deeper PSCz catalogue and see whether we can improve the agreement between the gravity field and the measured velocities, thus reducing the uncertainties in the estimate of β_I.

In Section 2 we review the basics of the VELMOD technique and describe its current implementation. The SFI sample is presented in Section 3 and the IRAS PSCz catalogue and its gravity field are described in Section 4. VELMOD is tested in Section 5 and the results of its application to the SFI catalogue are presented in Section 6. An analysis of errors based on the magnitude and velocity residuals is performed in Section 7. Finally, in Sections 8 and 9 we discuss the results and conclude.

2 THE VELMOD METHOD

VELMOD is a maximum likelihood method introduced by V1 and described in detail in V1 and V2. Here we simply outline the main points of the method, focusing on its implementation in the case of a forward TF relation. In Strauss & Willick's (1995) terminology, VELMOD uses a Method II approach, i.e. takes the TF observables (apparent magnitude and velocity width) and the redshift of an object and quantifies the probability of observing the former given the latter, for a particular model of the velocity field and a TF relation. This probability is then maximized with respect to the free parameters of the velocity model and the TF relation. Unlike previous Method II implementations (e.g. Hudson 1994), VELMOD replaces the redshift-distance relation with a joint probability distribution of distance and redshift. This probabilistic approach allows a statistical treatment of all those effects (small-scale velocity noise, inaccuracy of the velocity model and existence of triple-valued regions) that spoil the uniqueness of the redshift-distance mapping.

VELMOD does not require smoothing of the TF data which, along with the allowance for triple-valued regions and small-scale velocity noise, allows one to probe the velocity field in high-density regions, thus exploiting the denser sampling of the new PSCz galaxy catalogue. Another convenient feature of VELMOD is that it does not require an *a priori* calibration of the TF relation, which is a common issue of concern in peculiar velocity studies. Instead, a fit of the parameters of the TF relation is performed simultaneously with the parameters of the velocity field.

2.1 Implementation of VELMOD

For each galaxy, the angular position (l, b), redshift (cz), apparent magnitude (m), and velocity width parameter $(\eta \equiv \log_{10}(W) - 2.5$, where W is twice the rotation velocity of the galaxy) are taken from the SFI catalogue. Hereafter, we will always use the redshift measured in the Local Group (hereafter LG) frame unless otherwise specified. In addition, a model for the density field is needed to account for inhomogeneous Malmquist bias. Such a model is obtained from the distribution of IRAS PSCz galaxies, together with a self-consistent model for the peculiar velocity field (as described in Section 4). The velocity model is completely specified by the value of the β_I parameter and a one-dimensional velocity dispersion, σ_v, which quantifies both the inaccuracy of the velocity model and the true velocity noise arising from small-scale nonlinear motions. Strauss, Ostriker & Cen (1998) and V2 have shown that the velocity dispersion on small scales is an increasing function of the local density. The SFI galaxy sample considered in this work consists of field spirals which avoid high-density environments and thus we ignore such dependency and assume a constant σ_v, independent of the environment.

The probability of observing a magnitude m for a galaxy with a given η and distance r is modeled by a linear TF relation,

$$m = M(\eta) + 5\log(r) = A_{TF} - b_{TF}\eta + 5\log(r) + \sigma_r, \quad (3)$$

where σ_r is a Gaussian random distribution with zero mean and dispersion σ_{TF}. This TF relation is completely specified by its zero point (A_{TF}), slope (b_{TF}) and scatter (σ_{TF}). In this work we do not model a possible dependency of the TF scatter on the luminosity or velocity width. In section 6.4, we will find that our results are insensitive to this approximation.

The final ingredient needed to compute the probability of observing the measurements of the SFI catalogue are the selection function of the observational quantities and their correlations. Systematic errors can affect peculiar velocities computed with the forward TF relation if selection effects are not propery accounted for. For that purpose, we have used the correlation and selection models of Freudling *et al.* (1995).

With the above assumptions, one can compute the probability that the i-th object of the sample with recession velocity cz_{LG} and velocity width parameter η will have an apparent magnitude m: $P_i(m|\eta, cz_{LG})$. To evaluate this conditional probability one needs to integrate the joint probability distribution $P_i(m, \eta, cz_{LG})$ over m. Although analytic approximations for this integral have been introduced by V2, which are valid away from triple-valued regions and at distances much larger than σ_v, in this work we perform an explicit numerical integration for all galaxies.

From the overall probability, which we obtain by multiplying the single-object probabilities $P = \prod_i P_i(m|\eta, cz_{LG})$, we compute the likelihood $\mathcal{L} \equiv -2\ln P$ which is then minimized at each of 19 values of $\beta_I = 0.1, 0.15.....0.95, 1.0$ by continuously varying the remaining free parameters (i.e. the three TF parameters and σ_v). The function $\mathcal{L}_{min}(\beta_I)$ obtained by this procedure is then fitted with a cubic function and the maximum-likelihood value of β_I, β_{min}, is found at the minimum of the curve. Extensive tests with mock catalogues performed by V1 have shown that β_{min} is an unbiased estimator of the true β_I parameter.

V1 and V2 found systematic residuals between the IRAS 1.2Jy predicted and the Mark III observed velocities which they modeled as a velocity quadrupole with a distance-dependent amplitude. This quadrupole, which they treated as a free parameter in their VELMOD analysis, is likely to arise from the missing contributions to the model velocity field from the mass distribution in the regions beyond the limits of the IRAS 1.2Jy survey and from shot noise. The PSCz survey should be deep and dense enough to reduce such discrepancies allowing us to drop this extra parameter. Therefore, we choose not to allow for any external contribution to the PSCz velocity field in our VELMOD analysis. In Section 7 we will show that the PSCz velocity model within 6000 $\mathrm{km\,s^{-1}}$ does indeed constitute an acceptable fit to the SFI peculiar velocity field, with no need to introduce external contributions. Finally, unlike V1 and V2, we do not model the uncertainties in the LG velocity as a free parameter. Instead, we shall test explicitly the robustness of our results by running a few VELMOD experiments in which the LG velocity is allowed to vary within its 1-σ error range.

3 THE SFI SAMPLE

The SFI sample of galaxies (Giovanelli *et al.* 1997a; Haynes *et al.* 1999a,b) is a homogeneous all-sky sample of galaxies for which I-band Tully-Fisher parameters are available. The sample uses new observations for declinations $\delta > -40^\circ$ and re-reduced data from Mathewson, Ford and Buchorn (1992) in the southern polar cap. The sample is, by design, angular diameter limited, with different limiting diameters, D_{lim}, for different redshift shells. The limiting diameters, expressed in unit of 0.1 arcmin, are $D_{lim} = 25, 16$ and 13 in the redshift ranges $cz_{LG} < 3000\,\mathrm{km\,s^{-1}}$, $3000 < cz_{LG} < 5000\,\mathrm{km\,s^{-1}}$ and $5000 < cz_{LG} < 7500\,\mathrm{km\,s^{-1}}$, respectively. However, for a number of different reasons, some bright galaxies smaller than the stated diameter limit were included in the sample. These additional galaxies, which amount to $\sim 15\%$ of the total, do not constitute a strictly magnitude-limited sample. All of them are brighter than an apparent Zwicky magnitude of $m_z = 14.5$. In a detailed investigation of these extra galaxies, we have not found any dependence of the selection on distance or apparent diameter. This is different from the distance-dependent selection function that Willick *et al.* (1996) have used to describe the MAT sample. For the present analysis, we have therefore approximated the SFI selection sample as the combination of a strictly diameter-limited sample with the above criteria, and a magnitude-limited sample with limiting Zwicky magnitude of 14.5. For such a case, Willick

(1994) has derived the VELMOD formalism. In his terminology, this is the *Two-Catalogue Selection* case and the selection function, expressed in a form suitable for the VELMOD analysis, is given by eq. (63) of Willick (1994). We have found that the results presented in this paper do not change significantly when using $m_z = 13.5$ for the putative magnitude limit of the extra bright galaxies

Freudling *et al.* (1995) have modeled the correlations between the quantities used to define the selection criteria, (m_z, D), and the TF observables, (m_I, η), as

$$m_z = 1.6 + m_I + 0.5\eta \qquad \text{with dispersion } \sigma_{m_z} = 0.59 \tag{4}$$

and

$$D = 3.82 + -0.205 m_I - 0.102\eta \text{ with dispersion } \sigma_D = 0.121, \tag{5}$$

where m_I indicates the I-band apparent magnitude. These correlations can be easily translated into the VELMOD formalism.

Below, we will consider the following sub-samples drawn from the SFI catalogue. Most of the analysis is carried out with the 989 galaxies with $cz_{LG} < 6000\,\mathrm{km\,s^{-1}}$ and $\eta > -0.25$. These cuts allow us to perform a homogeneous comparison with the ITF analysis of D98. In addition, we will consider separate subsamples restricted to three independent redshift-space shells 2000 $\mathrm{km\,s^{-1}}$ thick and with external radii of 2000, 4000 and 6000 $\mathrm{km\,s^{-1}}$. These subsamples mix different nominal selection criteria and serve as an additional check that selection effects are well accounted for. The three subsamples contain 158, 355 and 496 galaxies, respectively.

SFI galaxies avoid rich clusters and high density environments. In particular none of them belong to the Virgo cluster. Therefore, there is no need to adopt any grouping procedure and the hypothesis of a small-scale velocity dispersion, σ_v, independent of the environment is well justified.

4 MODEL DENSITY AND VELOCITY FIELDS FROM THE PSCz SURVEY

The models for the density and velocity fields are obtained from the distribution of IRAS galaxies in the recently completed PSCz all-sky redshift survey (Saunders *et al.* 2000). This catalogue, which basically extends the old 1.2 Jy one (Fisher *et al.* 1995), contains ~ 15500 IRAS PSC galaxies with a flux at 60 μm larger than 0.6 Jy. A complete description of the dataset, its selection criteria, the procedures adopted to avoid stellar contamination and galactic cirrus, are given in Saunders *et al.* (2000). For our purposes, the most interesting features of the catalogue are the large area sampled ($\sim 84\%$ of the sky), its depth (the median redshift is 8500 $\mathrm{km\,s^{-1}}$) and dense sampling (the mean galaxy separation at 10000 $\mathrm{km\,s^{-1}}$ is $\langle l \rangle \sim 1000$ $\mathrm{km\,s^{-1}}$,* compared with a value of $\langle l \rangle \sim 1500$ $\mathrm{km\,s^{-1}}$ for the IRAS 1.2 Jy catalogue).

The flux-limited nature of the catalogue causes the number of objects to decrease with distance. This decrease is quantified by a radial selection function. Various authors have used different estimators to compute the selection function (Springel 1996, Canavezes *et al.* 1998, Sutherland *et al.* 1999, Branchini *et al.* 1999, Monaco and Efstathiou 1999, Saunders *et al.* 2000). Branchini *et al.* (1999, hereafter B99) found that different selection functions induce variations smaller than 5% in the model density and velocity fields within a distance of 20000 $\mathrm{km\,s^{-1}}$. In this work we use the selection function specified by eqn. (1) of B99.

The density and velocity field in real space are obtained from the redshift space distribution of PSCz galaxies by implementing *Method 1* of B99, which uses the iterative technique of Yahil *et al.* (1991) to minimize redshift-space distortions. The procedure relies on gravitational instability theory, assumes linear biasing, and is valid in the limit of small density fluctuations where linear theory applies. At each step of the iteration the gravity field, $\mathbf{g}$, is computed from the distribution of the 11206 PSCz galaxies within 20000 $\mathrm{km\,s^{-1}}$. The gravity field is subsequently smoothed with a top hat filter of radius ~ 500 $\mathrm{km\,s^{-1}}$ which allows us to assume linear theory and thus to obtain the smoothed

* Throughout this paper we measure distances in velocity units ($\mathrm{km\,s^{-1}}$). This is equivalent to setting the Hubble constant equal to unity.

peculiar velocity of each galaxy from the acceleration, $\mathbf{v} \propto \beta_I \mathbf{g}$. The new distances of the objects, r, are then assigned assuming a unique redshift–distance relation $r = cz - u$, where u is the radial component of the peculiar velocity vector. The procedure is repeated until convergence is reached.

The final products are the real space positions of the galaxies and their velocities for a given value of β_I. We have ran 19 different reconstructions with $\beta_I = 0.1, 0.15.....1.0$. The continuous density field is obtained by smoothing the galaxy distribution on 129^3 points of a cubic grid inside a box of 19200 $\mathrm{km\,s^{-1}}$ a side with the LG at the centre, using a Gaussian filter of 300 $\mathrm{km\,s^{-1}}$ (G3, hereafter). The associated smoothed velocity fields are computed for the appropriate value of β_I from eqn. (1).

The procedure returns 19 models of the density field (one for each value of β_I), along with their associated peculiar velocity fields, both defined at the gridpoint positions. Velocity predictions are made in the LG frame to minimize the uncertainties derived from the lack of information about the mass distributions on scales larger than the size of the PSCz sample.

5 TESTING THE VELMOD IMPLEMENTATION

In this work we rely on the error analysis performed by V1, based on an extensive application of VELMOD to realistic mock catalogues, which we do not repeat here. Instead, we present the results of two tests aimed at checking the reliability of our VELMOD implementation.

5.1 Tests with Ideal PSCz and SFI Mock Catalogues

As a first test, we applied VELMOD to a suite of SFI and PSCz mock catalogues. Errors in the VELMOD analysis are dominated by inhomogeneous Malmquist bias, with uncertainties in the model velocity fields playing an important role only in the innermost part of the sample. To account properly for Malmquist bias, the mass distribution in the mock catalogues needs to mimic the one in our local universe as close as possible. Unlike V1, however, we do not extract mock catalogues from constrained N-body simulations (i.e. similar to those produced by Kolatt *et al.* 1996). Instead, we construct 'ideal' PSCz and SFI mock catalogues from the G3 smoothed PSCz density and reconstructed linear velocity fields (described in the previous section) for $\beta_I = 1.0$. Nonlinear effects were mimicked by adding a constant Gaussian noise of 150 $\mathrm{km\,s^{-1}}$ to each of the Cartesian components of the model velocity vectors. Such a small value is meant to mimic the observed "coldness" of the cosmic velocity field (e.g. Strauss, Ostriker and Cen 1998).

Twenty mock PSCz catalogues where generated with Montecarlo techniques using different random seeds. Selection criteria close to the observational ones were applied to mimic the PSCz selection function and the presence of unobserved regions. Mock PSCz galaxies were generated assuming a probability proportional to the local density, i.e. assuming that they trace the mass distribution ($b_I = 1$). The same reconstruction method used for the real data was then applied to each of these mocks to obtain 20 mock PSCz velocity models for each of the 20 values of $\beta_I = 0.5, 0.55.....1.5$.

Similarly, we generate 20 mock SFI catalogues by Montecarlo resampling the original PSCz G3–smoothed density and velocity fields with the added thermal noise. First, catalogues with large numbers of galaxies were created. Next, absolute magnitudes were assigned according to the luminosity function. Subsequently, diameters and velocity widths were assigned according to the correlations described in Section 3. TF parameters close to the ones found in our final analysis were used to assign velocity widths. Finally, the nominal selection criteria of the SFI sample were used to select galaxies for the final catalogues. The additional galaxies mentioned in Section 3 were simulated by randomly including galaxies up to the magnitude limit until the number of galaxies not satisfying the nominal selection criteria matched the one of the SFI sample. The resulting mock samples nicely reproduce the observed redshift distribution of the SFI sample.

The results of applying VELMOD to the 20 SFI mock catalogues are summarized in table 1. The true values of the free parameters used in the mock catalogues are listed in the first row while those obtained from the VELMOD

analysis are shown in the second row. For each parameter we report the average value from the 20 mocks, the error in the mean and, in parenthesis, the typical error in a single realization. These results indicate that VELMOD returns an unbiased estimate of the free parameters.

Given the ideal nature of the velocity field in these mock catalogues the errors displayed in table 1 are likely to underestimate the real ones. In what follows, however, we will be mainly interested in the errors on β_I which, as V1 demonstrated, can be obtained from the values at which $\mathcal{L}_{min}(\beta_I)$ differs by one unit from its minimum value at β_{min}.

5.2 Tests with the Mark III Catalogue

In the second test, we repeated part of the VELMOD analysis performed by V1 and V2, but using the PSCz model velocity field instead of the IRAS 1.2 Jy one. We applied VELMOD to the Aaronson *et al.* (1982, hereafter A82) and Mathewson *et al.* (1992, MAT) subsamples selected according to the V1 prescriptions. The selection functions for A82 and MAT and their coefficients were taken from Willick *et al.* (1996). Both samples are spatially limited to a redshift $cz_{LG} = 3000\,\mathrm{km\,s^{-1}}$. A third subsample we use, MAT2, also obtained from the Mathewson *et al.* (1992) catalogue, coincides with the one considered by V2 and extends out to $cz_{LG} = 7500\,\mathrm{km\,s^{-1}}$.

The results are summarized in table 2 where the values of the free parameters obtained from our VELMOD analysis are compared to those obtained by V1 and V2 (in parenthesis). Only errors in β_I are quoted. Our results generally agree with those of V1 and V2. The analysis of the MAT and MAT2 samples returns values of β_I smaller than those obtained by V1 and V2. The difference is within the 1σ error bar and probably reflects the difference between the IRAS 1.2 Jy and PSCz model velocity fields.

The largest discrepancy is the σ_v parameter for which we consistently obtain values larger by $30-70\%$ than those estimated by V1 and V2. Such discrepancy is statistically significant since the expected errors on σ_v estimated from the mock catalogues and, more qualitatively, from the likelihood curve, are of the order of 40 $\mathrm{km\,s^{-1}}$. To interpret this discrepancy one has to keep in mind that the value of σ_v is approximately given by the sum in quadrature of random velocity noise (σ_T) and the uncertainties in the model velocity field (σ_M).

The only possible explanation for the discrepancy in σ_v is that σ_T, which is an intrinsic property of the velocity catalog, is the same in both analyses, but the PSCz velocity model has a larger σ_M. Indeed, since B99 estimate $\sigma_M \sim 130\,\mathrm{km\,s^{-1}}$ for the PSCz model, while V1 find $\sigma_M \sim 84\,\mathrm{km\,s^{-1}}$ for the IRAS 1.2Jy model, one may think that the intrinsic velocity noise would then be similar in the PSCz ($\sigma_T \sim 120\,\mathrm{km\,s^{-1}}$) and IRAS 1.2Jy ($\sigma_T \sim 100\,\mathrm{km\,s^{-1}}$). However, it is difficult to understand why errors in the PSCz model should be larger than in the IRAS 1.2Jy one. The denser sampling and larger depth of the PSCz catalogue should decrease the uncertainties in the model velocity field, not increase them. In fact, the errors quoted by V1 and B99 were estimated using different mock catalogues. V1 used mocks derived from the reconstruction technique of Kolatt *et al.* (1996) which are based on a PM N-body code and are intrinsically "colder " than those used by B99 which were taken from the higher resolution AP^{3}M N-body simulations of Cole *et al.* (1998). Since the precision of the velocity reconstruction decreases with increasing small-scale random velocity noise, it is reasonable to suspect that the difference in the values of σ_M estimated by V1 and B99 simply reflects the differences in the mock catalogues rather than differences in the errors of the two model velocity fields, and that an error analysis based on the same set of mock catalogs would show that the value of σ_M for the PSCz model is comparable, if not smaller, than for the IRAS 1.2Jy model velocity field.

Nevertheless, the σ_v discrepancy must reflect some difference in the IRAS PSCz and 1.2Jy velocity prediction. The only remaining possibility is that such a difference is systematic rather than purely random. Indeed, the two models are different because they are based on two different redshift catalogues and because they are derived using two different reconstruction methods. The PSCz catalogue allows a denser sampling and therefore traces small-scale density fluctuations which are washed out by shot noise in the IRAS 1.2Jy catalogue. The IRAS 1.2 Jy model used by V1 and V2 was obtained using the technique of Sigad *et al.* (1998) which differs from the one of B99 in the treatment of triple-valued regions, the use of Wiener filtering, and, most importantly, in the allowance for mildly nonlinear motions. As a result, the PSCz velocity model is intrinsically more linear than the IRAS 1.2Jy one which

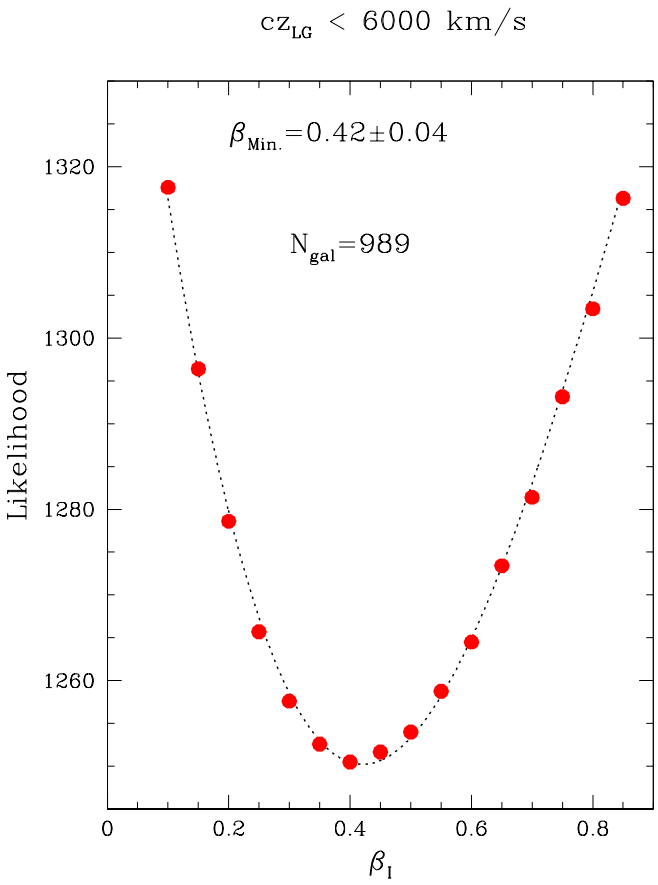

Figure 1. The VELMOD likelihood , $\mathcal{L}_{min}(\beta_I)$, (filled symbols) for the full SFI sample. The dotted curve represents a cubic fit to the points.

also lacks power on small scales. The linearity of the PSCz model forces any discrepancy between true and model velocities to contribute to σ_v. In the IRAS 1.2Jy case, such discrepancies are, on average, smaller because of the lack of small-scale power and because they are partially absorbed by the mildly nonlinear motions. The net result is that VELMOD analyses based on the IRAS 1.2 Jy velocity model return values of σ_v systematically smaller than those based on the PSCz velocity model and a value of β slightly larger.

6 RESULTS

In this section we present the results of applying the VELMOD analysis to the SFI sample within 6000 km s^{-1} and we check the robustness of our results using smaller subsamples, smoothing scale and errors in the LG velocity.

6.1 Application to the Full SFI Catalogue

We ran VELMOD on the full SFI sample of 989 galaxies with redshift $cz_{LG} < 6000$ km s^{-1} and $\eta > -0.25$. The PSCz density and velocity fields used in this calculation were smoothed with a Gaussian filter of effective radius 300 km s^{-1}. The likelihood was minimized at each of 19 values of $\beta_I = 0.1, 0.15, ...1.0$ by varying the free parameters A_{TF}, b_{TF}, σ_{TF} and σ_v. The resulting values of $\mathcal{L}_{min}(\beta_I)$ are represented by filled dots in fig 1. In order to find the actual minimum, we fit a cubic function to $\mathcal{L}_{min}(\beta_I)$:

$$\mathcal{L}_{min} = \mathcal{L}_0 + a_1(\beta_I - \beta_{min})^2 + a_2(\beta_I - \beta_{min})^3 \quad (6)$$

The value of β_{min} and its errors are indicated in the plot and are also listed in table 3 together with the values of the other parameters found at the minimum of the likelihood curve.

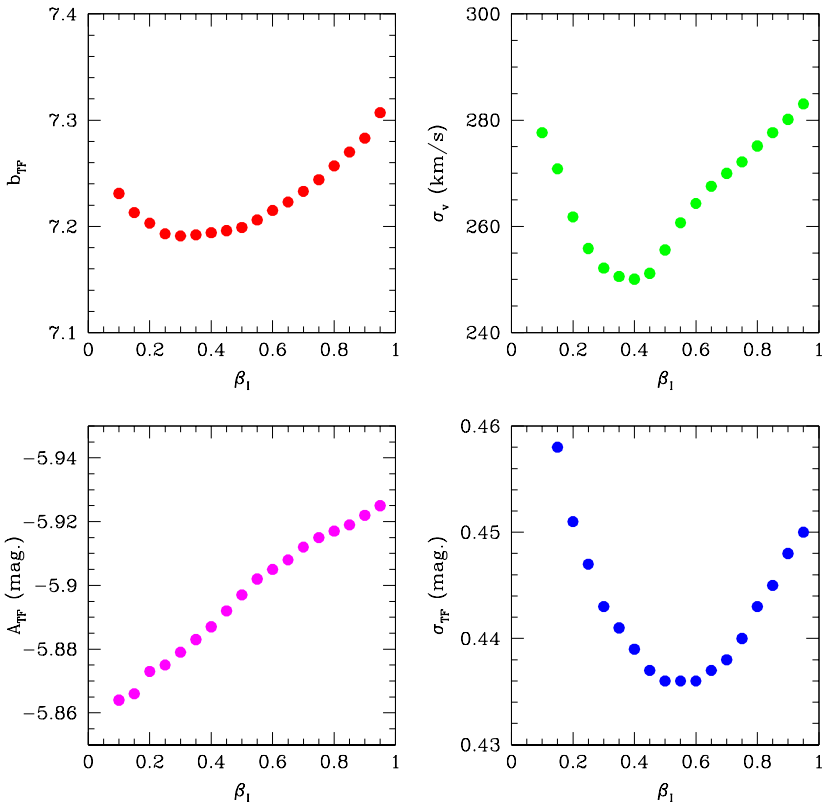

Figure 2. Best fit parameters obtained from running VELMOD on the full sample as a function of β_I: TF slope (top left), TF zero point (bottom left) velocity dispersion (top right) and TF scatter (bottom right).

The values for the TF parameters listed in table 3 should be compared with the values found by Giovanelli *et al.* (1997b, G97) for an associated sample of cluster galaxies, termed SCI, selected in a similar way to the SFI sample, which are commonly used as the assumed TF relation for the SFI sample. They find zero point, A_{TF}, of -6.00 ± 0.02[†] and slope, b_{TF}, of 7.5 ± 0.2 with a scatter of about 0.36 magnitudes. While the range of values for the slope of this determination from cluster galaxies overlaps with the current results, we obtain a smaller value for the zero point and a larger scatter. This is in agreement with other analyses of the SFI dataset (D98, Freudling *et al.* 1999). A similar difference in the TF scatter of cluster and field samples has been found in other datasets (e.g. Bothun & Mould 1987; Freudling, Martel & Haynes 1991).

The recovered value of $\sigma_v = 250$ km s^{-1} is twice as large as the value obtained by V1 and V2. As we have already discussed, part of this discrepancy may simply reflect differences between our model velocity field and the one used by V1 and V2. It may also indicate that the PSCz velocity model does not provide a satisfactory fit to the SFI dataset. We will return to this important point in Section 7.

Figure 2 shows the variation of the four parameters with β_I, where the other parameters are allowed to vary. The velocity dispersion reaches a minimum when $\beta_I \sim \beta_{min}$, a behavior consistent with the analysis of the mock catalogues performed by V1 (but not with their analysis of the real A82+MAT sample). The TF parameters are very insensitive to β_I. The largest variation ($\sim 5\%$) occurs for the TF scatter which has a minimum around $\beta_I = 0.55$, significantly larger than β_{min}. This is not alarming since, as stressed by V1, minimizing the TF scatter does not correspond to maximizing the likelihood. This is probably due to the covariance between σ_v and σ_{TF}: the increase of σ_v after its minimum is compensated by a further decrease of σ_{TF}.

[†] In this work absolute magnitudes refer to distances in units of km s^{-1}, and not of 10 pc, as often adopted in the literature

6.2 The Effect of Smoothing

In their analysis, V1 noticed that smoothing the model velocity field with a G5 filter had little effect on the VELMOD results. Along with their small value of σ_v, this was taken as an indication that density fluctuations on scales between 300 and 500 $\mathrm{km\,s^{-1}}$ contribute little to both the Mark III and the IRAS 1.2Jy velocity fields. However, the larger value of σ_v we have found in our VELMOD analysis of the A82, MAT and SFI samples seems to indicate that contributions from small scales are non-negligible.

To investigate this issue, we have repeated the same exercise and performed a VELMOD analysis using a G5 smoothed PSCz model velocity field instead of the G3 one. We find that the results are insensitive to the smoothing scale, with β_{min} increasing only by $\sim 5\%$, consistent at the 1σ level with the value found in the G3 case. The same is true for the other free parameters with the exception of σ_v which increases by $\sim 15\%$. Moreover, the value of $\mathcal{L}_{min}$ at β_{min} increases by 10 units with respect to the G3 case, corresponding to a probability decrease by a factor $e^5 \simeq 90$ (as $\mathcal{L} = -2\ln P$). How do we interpret these results ? With a G5 filter, the model velocity field does not receive contributions from scales smaller than ~ 500 $\mathrm{km\,s^{-1}}$ and larger values of β_I and σ_v are needed to match the amplitude of the observed velocities. This means that the linear PSCz model velocity field does receive a non-negligible contribution from small scales. The significant increase in the likelihood indicates that the G3 velocity field provides a better fit to the SFI velocities, i.e. small-scale fluctuations do contribute to the peculiar velocities of galaxies in the real world.

6.3 Uncertainties in the Velocity of the Local Group

Since model predictions are given in the LG frame (i.e. the LG velocity is subtracted from all other velocities), we need to quantify the impact of uncertainties in the predicted and measured LG velocity when performing the VELMOD analysis. V1 and V2 tackled the problem by introducing a free parameter to model a random component to the LG velocity vector. Here we take a different approach aimed at minimizing the number of free parameters in the analysis. Instead of modeling the uncertainties in the LG velocities, we quantify the impact that these uncertainties, independently estimated, may have on our VELMOD analysis. Errors in the LG velocity derive from uncertainties in modeling the LG velocity and in transforming redshifts from the heliocentric to the LG frame. The former have been quantified by Schmoldt *et al.* (1999), while for the latter we consider the recent work of Courteau & van den Bergh (1999). We assume that these error estimates are independent and so we compute the total uncertainty by adding them in quadrature. The resulting total error in the LG velocity is $\sim 120\beta_I$ $\mathrm{km\,s^{-1}}$ for each Cartesian component.

To evaluate the impact of these errors we ran 10 VELMOD analyses in which the LG velocity was perturbed with a Gaussian noise of the same amplitude. The effect is to increase the random errors without introducing any systematic bias. Averaging over the 10 experiments we obtain a value of $\beta_I = 0.43$ with a 1-σ error around the mean of 0.05, slightly larger than the typical error in a single realization. Similar considerations apply to the other parameters. In all but one experiment the value of $\mathcal{L}_{min}(\beta_{min})$ was larger than in the unperturbed case. In the one case with smaller likelihood (by only two units) the perturbation turned out to be very small, in agreement with the V1 and V2 results in which the extra random components added to the LG velocity vector turned out to be trivially small.

6.4 Breakdown by Rotation Velocities

In their calibration of the TF relation for SCI galaxies, G97 found that the TF scatter is a function of the velocity width: rapidly rotating galaxies have a smaller TF scatter than slow rotators. A similar trend has also been detected by Federspiel, Sandage & Tamman (1994) and by Willick *et al.* (1997a) in some of the Mark III subsamples. In the SFI catalogue itself this effect has been included for the direct TF relation by Freudling *et al.* (1999), but not in the inverse TF relation (D98). In the current analysis, we have chosen to neglect this effect. To estimate the impact of this approximation we divided the SFI catalogue into two subsamples according to the rotational velocity of the galaxies. In the first catalogue, we included only objects with a velocity width parameter $\eta > -0.1$, while in the

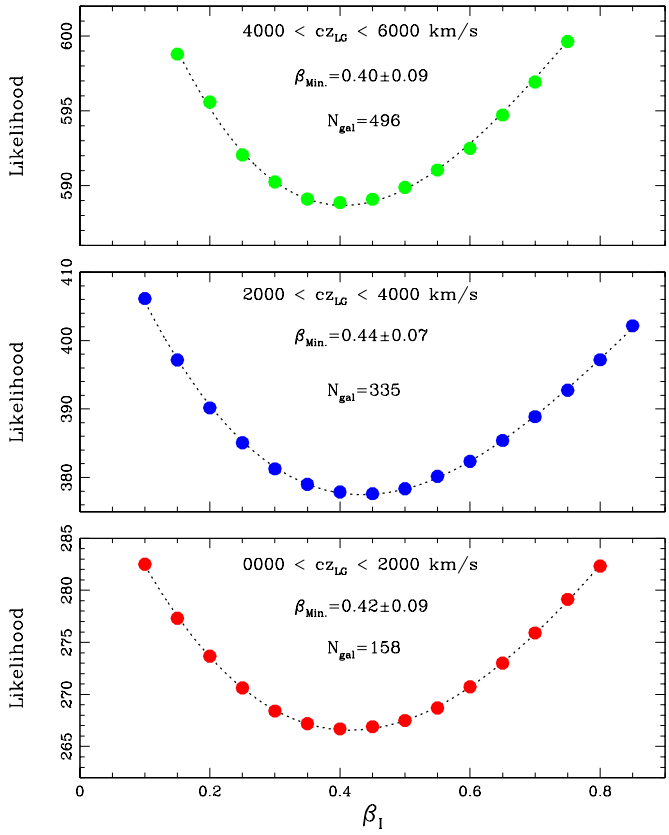

Figure 3. Likelihood curves, $\mathcal{L}_{min}(\beta_I)$, for three different redshift intervals. In each case the value of β_{min} and the number of galaxies in the samples are indicated. The dotted curves are cubic fits to the $\mathcal{L}_{min}(\beta_I)$ points.

second we included slow rotators with $\eta < -0.1$. The results of applying VELMOD on these two samples are shown in table 3. The TF dispersion is found to be smaller for fast rotators, as could be expected. However, the values of the other free parameters, in particular β_{min}, are very similar in the two subsamples, showing that our approximation of a constant σ_{TF} has little impact on our β_I estimates.

6.5 Breakdown by Redshift

As a last robustness test we have divided our sample into three independent redshift shells 2000 $\mathrm{km\,s^{-1}}$ thick and applied VELMOD to each of them. Since the selection criteria are different in the three shells, this test serves as a check of whether selection effects are properly taken into account by our procedure. The resulting $\mathcal{L}_{min}(\beta_I)$ curves are displayed in fig. 3 and the free parameters are listed in table 3. The values of β_{min} in the three shells are consistent with each other. The remaining parameters are also in good agreement, with only two exceptions. One is the TF slope which in the innermost shell is $\sim 10\%$ shallower than in the rest of the sample. The analysis of SFI mock catalogues in Section 5.1 reveals that such a discrepancy is significant at the 1.5σ level. However, as we have already pointed out, the errors estimated using those catalogues are smaller than the real ones. A VELMOD analysis of more realistic SFI mocks would return larger errors and decrease the statistical significance of the slope variation.

The second, more serious, discrepancy is observed for σ_v which in the outermost shell increases by a factor of ~ 2.7. Such a variation is much larger than what we observe in the mock catalogues and deserves some further investigation. We have therefore sliced the SFI sample into thinner redshift shells, all of them 1000 $\mathrm{km\,s^{-1}}$ thick except the innermost one which we extended to 2000 $\mathrm{km\,s^{-1}}$ so that a comparable number of objects is contained in each shell. We then repeated the VELMOD analysis in each of these shells. The results are visualized in the histograms of fig 4. The two dashed lines represent the 1σ error about the mean. The upper plot shows the radial behaviour of σ_v. Within 4000 $\mathrm{km\,s^{-1}}$, $\sigma_v \simeq 200$ $\mathrm{km\,s^{-1}}$, comparable to what we have obtained from the analysis of the

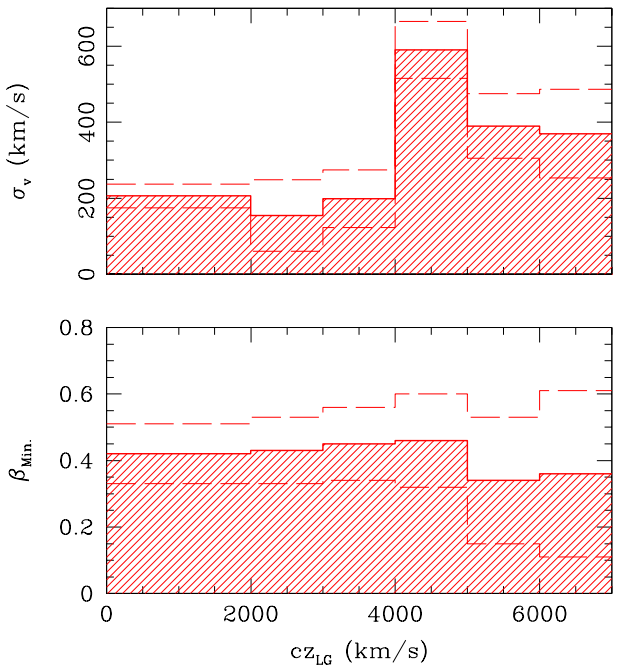

Figure 4. Dependency of σ_v (upper plot) and β_{min} (lower plot) on redshift. The histograms show the results of running VELMOD on 6 different redshift shells. In both plots the dashed lines represent 1σ errors around the mean.

A82, MAT and MAT2 samples. This value is larger than those found by V1 and V2 and, as discussed in Section 5.2, this is probably because the the PSCz model velocity field is more sensitive to power on small scales. Around 5000 km s^{-1} σ_v increases to ~ 600 km s^{-1} and then stabilizes at a value of ~ 400 km s^{-1}.

In order to test whether any particular part of the sky is responsible for this dependence of σ_v on distance, we have cut the sample into several complementary hemispheres (e.g. above and below the the Galactic plane, above and below the Supergalactic plane and so on) and, for each pair, we have ran VELMOD on the two sets of redshift shells. In all cases we have found that σ_v increases beyond 4000 km s^{-1}, suggesting that no particular cosmic structure is responsible for the increase in σ_v.

The ability of VELMOD to constrain σ_v is a rapidly decreasing function of the redshift and we need to assess the statistical significance of the jump at 4000 km s^{-1}, i.e. we need to estimate the errors on σ_v. We compute them from the distribution of σ_v found from the analysis of our 20 mock SFI samples. This test reveals that the increase of σ_v is significant at about the 3σ level, leaving little doubt about the reality of the change at around 4000 km s^{-1}. However, as we have already stressed, such tests are only indicative since non-linearities are not properly modeled in our mock samples.

To further assess the reality of this peak we performed a second test. We ran two VELMOD analyses using only objects with redshifts in the range 4000–6000 km s^{-1}. In the two calculations all the parameters were fixed to their maximum likelihood values except σ_v which was set equal to 200 km s^{-1} in one case and to 535 km s^{-1} (i.e. its maximum likelihood value) in the other. The smaller σ_v results in an increase of 12 units in the likelihood or a decrease in probability of $\sim e^6 \simeq 400$, indicating that the increase in σ_v seen in the external shell is indeed significant. It is therefore possible that the dramatic increase in σ_v reflects a disagreement between the velocity model and the SFI data on large scales. We will investigate this possibility further in the next section.

The lower plot of fig 4 shows how β_{min} varies with redshift. VELMOD returns a very robust estimate of β_{min} which does not change significantly even when σ_v increases. Despite this encouraging evidence, it is sensible to

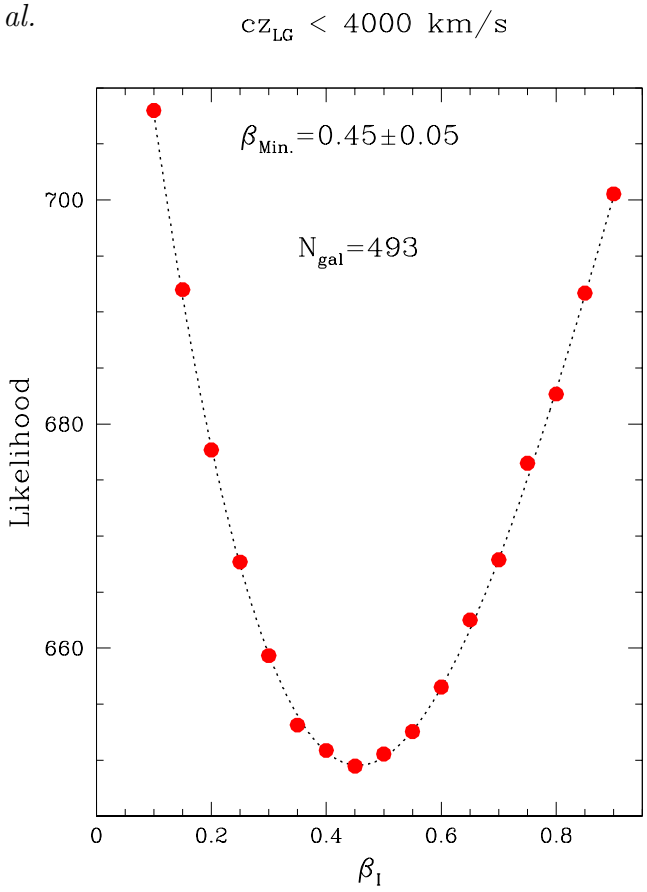

Figure 5. The VELMOD likelihood, $\mathcal{L}_{min}(\beta_I)$, (filled symbols) for SFI galaxies with $cz_{LG} < 4000$ km s^{-1}. The dotted curve represents a cubic fit to the points.

adopt a more conservative approach and repeat the VELMOD analysis within 4000 km s^{-1}, i.e. in the volume where there are no obvious indications of a possible mismatch between model and data. The results, listed in table 3, are in good agreement with those of the full sample. In particular, the minimum of the likelihood curve (shown in fig. 5), $\beta_{min} = 0.45 \pm 0.05$, is fully consistent with the results from the other subsamples. The velocity dispersion is ~ 200 km s^{-1}, in good agreement with those obtained from the analysis of the A82, MAT and MAT2 samples.

7 ANALYSIS OF THE VELOCITY AND MAGNITUDE RESIDUALS

VELMOD is a maximum likelihood technique in which the sources of variance, σ_v and σ_{TF}, are treated as free parameters. For this reason, the VELMOD analysis can only tell us which are the best values of β_I, A_{TF}, b_{TF}, σ_{TF} and σ_v for a given velocity field model, but it cannot address the question of whether the velocity model is an acceptable fit to the data. In this respect, the increase of σ_v at large radii found in the preceeding section is only suggestive of a mismatch between observed and modeled velocities, and a proper error analysis is needed to assess its statistical significance. In this section we address this problem by inspecting the magnitude and velocity residuals, following the formalism and notation of V1.

7.1 Maps of Velocity Residuals

We define the normalized magnitude residuals for each object of magnitude m:

$$\delta_m = \frac{m - E(m|\eta, cz)}{\Delta_m}, \tag{7}$$

where the expected apparent magnitude, $E(m|\eta, cz)$, and the dispersion around it, Δ_m, can be obtained by integrating over the constrained probability function, $P(m|\eta, cz_{LG})$, which is computed in the VELMOD analysis. The magnitude

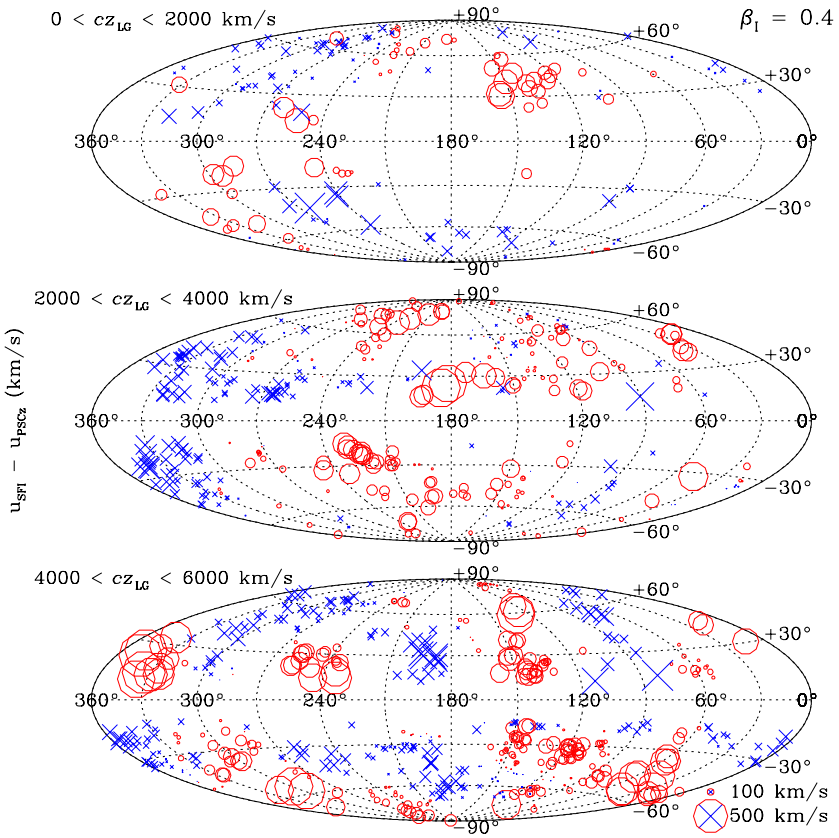

Figure 6. The sky projection in Galactic coordinates, as seen in the LG frame, of the smoothed VELMOD velocity residuals, $u_{SFI} - u_{\rm PSCz}$, for $\beta_I = 0.4$. Open circles indicate objects that are inflowing relative to PSCz velocity predictions; crosses denote objects that are outflowing. The size of the symbols is proportional to the amplitude of the velocity vector.

residuals where smoothed on a scale $S = d/5$, where d is the PSCz predicted distance of the generic object, and then converted into smoothed peculiar velocity residuals, $u_{SFI} - u_{\rm PSCz}$, according to the V1 prescriptions. The resulting maps of the velocity residuals are shown in figs. 6, 7 and 8 for three different values of β_I and in three different redshift shells. When looking at the maps one should bear in mind that coherence up to scales of $\sim 35^\circ$ is induced by the adopted smoothing and therefore systematic mismatches between the model and reality can only be revealed by coherence on much larger angular scales. The visual inspection of the maps clearly shows that the velocity residuals for $\beta_I = 0.4$ are less coherent and have smaller amplitudes than those of the models with $\beta_I = 0.1$ and $\beta_I = 1.0$. The residuals in the $\beta_I = 0.1$ map show a pattern similar to $\beta_I = 0.4$ case, but have a larger amplitude and coherence. When $\beta_I = 1.0$, the residuals grow even larger and the map exhibits a clear dipolar structure. The velocity residuals of the model with $\beta_I = 0.4$ look qualitatively similar to the ones between the SFI and IRAS 1.2Jy velocities for $\beta_I = 0.6$, as seen in fig. 7 of D98. However, a one-to-one comparison between the two sets of maps is not possible since different smoothing procedures were used and since our residuals are computed at the PSCz predicted distances whereas the ones of D98 are computed at the redshift space positions.

7.2 Residual Correlation Function

A more quantitative assessment of the goodness of fit can be obtained by computing the correlation function of the unsmoothed magnitude residuals:

$$\psi(\tau) = \frac{1}{N(\tau)} \sum_{i<j} \delta_{m,i} \delta_{m,j}, \tag{8}$$

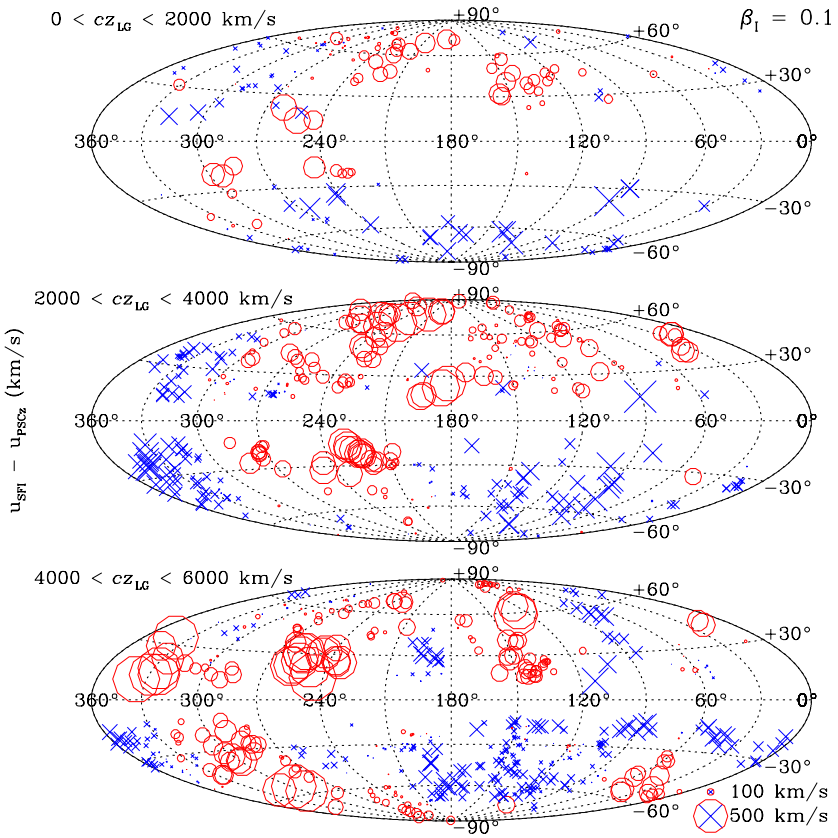

Figure 7. The sky projection of the smoothed VELMOD velocity residuals $u_{SFI} - u_{\rm PSCz}$ for $\beta_I = 0.1$.

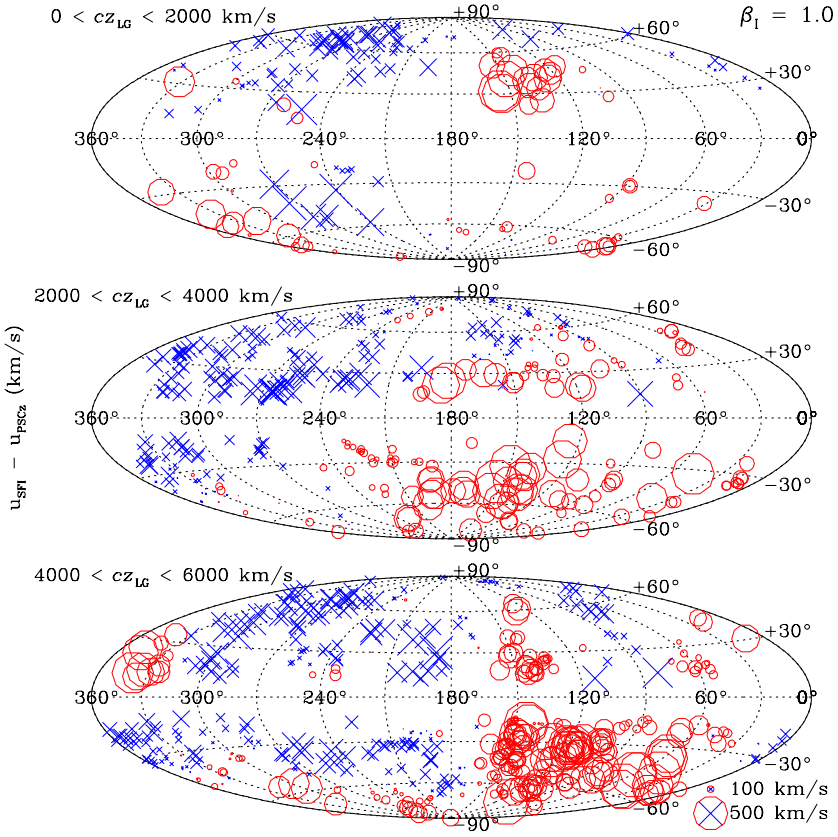

Figure 8. The sky projection of the smoothed VELMOD velocity residuals, $u_{SFI} - u_{\rm PSCz}$, for $\beta_I = 1.0$

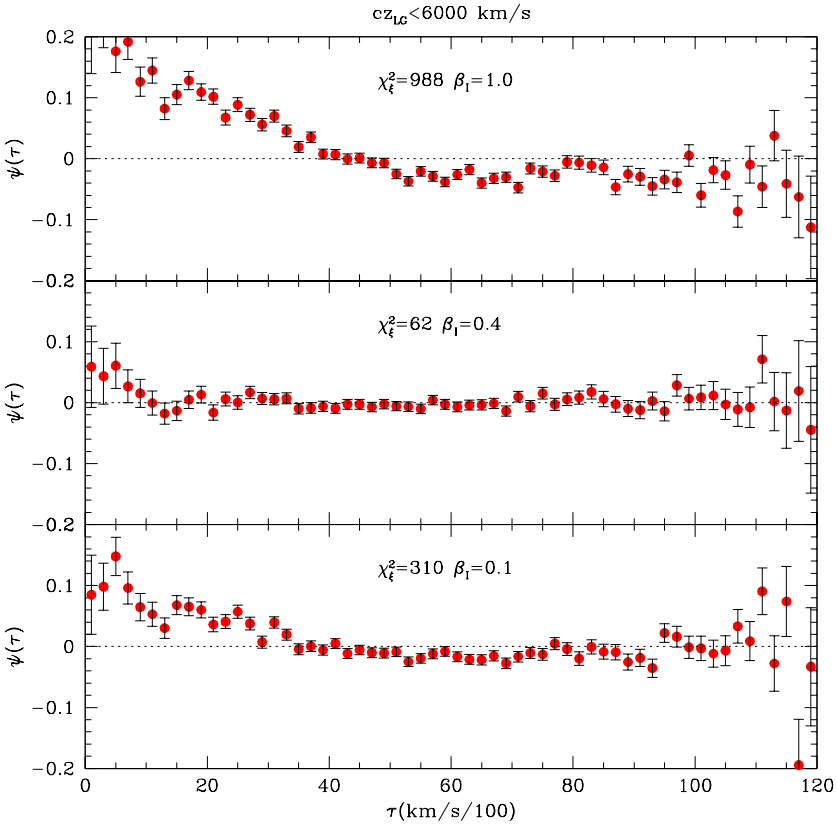

Figure 9. The correlation function of magnitude residuals plotted for $\beta_I = 0.1$ (lower plot), $\beta_I = 0.4$ (middle plot) and $\beta_I = 1.0$ (upper plot). The results refer to the full SFI sample.

where $N(\tau)$ is the number of galaxy pairs with predicted separation $d_{ij} \leq \tau \pm 100\,\mathrm{km\,s^{-1}}$. This correlation function applies to normalized magnitude residuals, i.e., does not depend on σ_v and σ_{TF} and is only sensitive to genuine correlation among residuals.

In fig. 9 we show the correlation function of all SFI galaxies with $cz_{LG} < 6000\,\mathrm{km\,s^{-1}}$ for the same three values of β_I used to produce the velocity residuals shown in figs. 6, 7 and 8. The error bars represent Poisson errors $N(\tau)^{-0.5}$. In the $\beta_I = 0.4$ model, the correlation function appears to be consistent with zero almost everywhere apart from some positive correlation at separations smaller than $500\,\mathrm{km\,s^{-1}}$, i.e. of the order of the smoothing scale of the model velocity field. A significant excess correlation on small and large scales is detected for $\beta_I = 0.1$ and, to an even greater degree, for $\beta_I = 1.0$.

To quantify the goodness of the fits we compute the quantity

$$\chi^2_\xi = \sum_{i=1}^{N_{bins}} \frac{\xi^2(\tau_i)}{N(\tau_i)}, \tag{9}$$

where $\xi(\tau) = N(\tau)\psi(\tau)$ and N_{bins} is the number of independent distance bins in which $\psi(\tau)$ is computed. V1 have shown that if the residuals are indeed uncorrelated on a scale τ then $\xi(\tau)$ is a Gaussian random variable with zero mean and variance $N(\tau)$. Under this approximation, the χ^2_ξ statistic is distributed as χ^2 with number of degrees of freedom equal to the number of independent distance bins. Any correlation among residuals will result in a larger χ^2_ξ. Extensive tests with mock catalogues performed by V1 revealed that χ^2_ξ indeed has properties similar to a χ^2 statistic, with the same variance, but with a mean of ~ 0.87 per degree of freedom rather than unity. We have computed the quantity χ^2_ξ for 10 values of β_I ranging from 0.1 to 1.0. The results are shown in fig 10. The continuous, heavy line shows the expectation value for a χ^2 statistic with $N_{bins} = 60$ degrees of freedom, while the dashed and long–dashed lines show, respectively, the 1σ and 3σ deviations from that value. The dotted line represents the expectation value of χ^2_ξ according to the V1 correction, i.e assuming a number of degrees of freedom of $0.87 \times 60 = 52.2$.

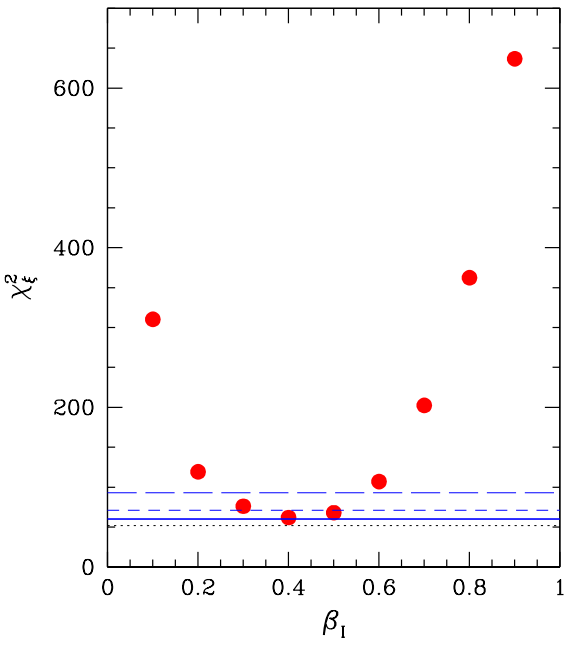

Figure 10. The statistic χ^2_ξ plotted for various values of β_I. The heavy line shows the expectation value for a χ^2 statistic with the same number of degrees of freedom. The dashed and long–dashed lines show 1σ and 3σ deviations from the expectation value. The dotted line shows the expectation value of χ^2_ξ corrected according to V1.

Despite its limited discriminatory power, the χ^2_ξ statistic clearly indicates that PSCz velocity models with $0.3 \leq \beta_I \leq 0.5$, and therefore also our best model according to the VELMOD analysis, $\beta_I = 0.42 \pm 0.04$, provide an acceptable fit to the SFI velocities. All other models with smaller or larger values of β_I can be ruled out at a level $> 3\sigma$.

We are now in a position to address the question of whether the PSCz model velocity field provides an acceptable fit throughout the whole SFI sample, particularly in the external regions where σ_v is large. We do that by computing the residual correlation function in the same three redshift shells previously used. The results are displayed in fig. 11 which shows the correlation functions, $\psi(\tau)$, for the three subsamples.

The value of $\psi(\tau)$ appears to be consistent with the null hypothesis of no correlation in nearly all the distance bins in each of the three redshift shells, with the exception of an excess correlation at small separation in the outermost shell. The value of the statistic χ^2_ξ in each shell is indicated in the plots. It is always smaller than the number of bins used in each shells and comparable to the expectation value for χ^2_ξ computed using the V1 correction. These results show that, despite the large value of σ_v obtained from the VELMOD analysis, the residuals of the fit are not correlated, i.e. the differences in magnitude between model and data are randomly distributed.

8 DISCUSSION

The results of our VELMOD analysis generally agree with those of independent analyses, with the exception of the velocity noise, σ_v. We find a significantly larger value than that found by V1 and V2 who compared the Mark III velocities to the IRAS 1.2Jy model velocity field. A VELMOD analysis of SFI subsamples limited in redshift revealed the existence of two regions. An inner sphere of radius 4000 $\mathrm{km\,s^{-1}}$ in which $\sigma_v \simeq 200$ $\mathrm{km\,s^{-1}}$, a value which is

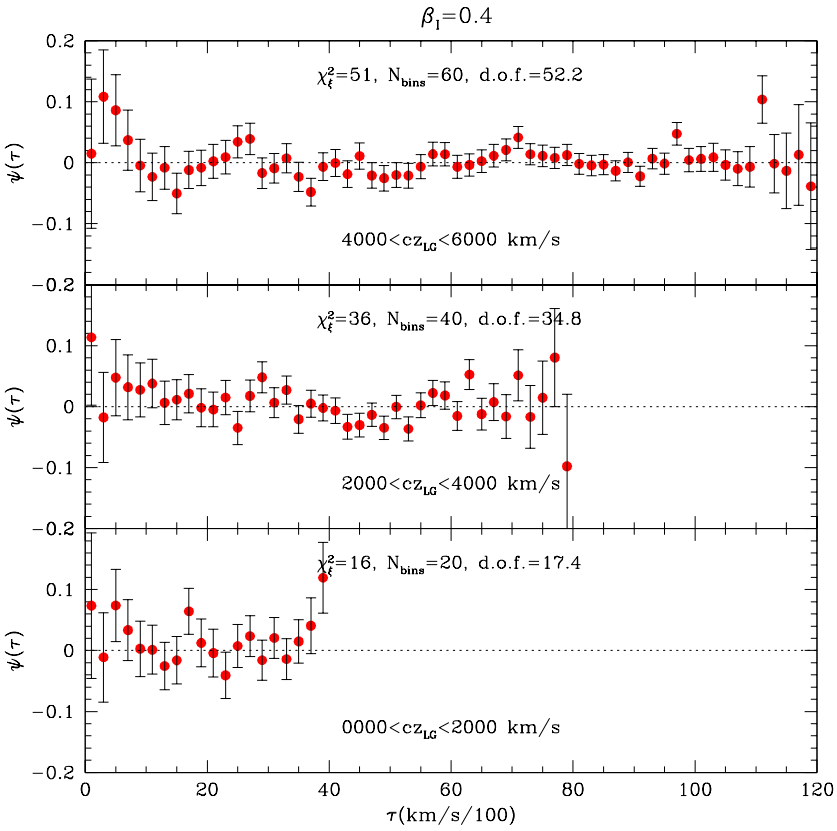

Figure 11. Residual correlation function in three redshift shells for the model $\beta_I = 0.4$. The redshift ranges, values of χ^2_ξ, number of bins and, in parenthesis, the number of degrees of freedom corrected according to V1 are also shown in the plots

believed to reflect the cumulative effect of velocity noise and errors in the model predictions (as corroborated by the results of the analysis of the A82 and MAT samples), and an external region in which $\sigma_v \sim 500\,\mathrm{km\,s^{-1}}$.

If these large values of σ_v were caused by systematic deviations of the SFI velocity field from the model predictions, then the residuals should correlate on scales larger than the smoothing length. However, this is not the case (see fig. 10). In fact, the residuals turn out to be quite small and do not show any significant spatial correlation. This is true for all redshift shells, including the outermost one where σ_v is large. Moreover, a quantitative analysis based on a χ^2 statistic shows that the PSCz velocity model with $0.3 < \beta_I < 0.5$ does provide a satisfactory fit to the SFI data without the need to introduce any external fields as in the V1 and V2 VELMOD analyses. This can be interpreted as implying that discrepancies between the model and the data do exist, but not in the form of peculiar motions coherent on scales larger than $\sim$ 300 $\mathrm{km\,s^{-1}}$. Rather, they are randomly distributed and thus properly quantified by means of the total variance, to which both σ_v and σ_{TF} contribute. It is worth noticing that the increase in σ_v occurs at the distance at which large structures like the Perseus-Pisces supercluster and the Great Attractor appear in the sample. Non-linear effects may be strongest in these structures, leading to a mismatch on small scales between measured and predicted velocity fields which could contribute to the increase in σ_v. To investigate whether these structures are indeed responsible for the increase in σ_v we have ran two VELMOD analyses in which we have excluded either SFI galaxies in the Perseus-Pisces supercluster (i.e. with $120^\circ \le l \le 170^\circ$, $-35^\circ \le b \le 5^\circ$ and $4000\,\mathrm{km\,s^{-1}} \le cz_{LG}$ $le6000\,\mathrm{km\,s^{-1}}$ or in the Hydra Centaurus region (i.e. with $260^\circ \le l \le 330^\circ$, $-10^\circ \le b \le 40^\circ$ and $2000\,\mathrm{km\,s^{-1}} \le cz_{LG} \le 6000\,\mathrm{km\,s^{-1}}$). A third analysis has been performed after excluding galaxies in both structures. The results turned out to be very similar to those shown in figure 4 for the full sample case (the differences are of the order of 20 $\mathrm{km\,s^{-1}}$). The abrupt increase of σ_v at $cz_{LG} \ge 4000\,\mathrm{km\,s^{-1}}$ is present in all the cases explored, showing that neither the Perseus-Pisces supercluster nor the Great Attractor contribute appreciably to the variation of σ_v.

A second possibility is that the increase in σ_v with redshift is caused by a comparable increase in the errors of

the velocity model. Indeed, B99 quantified such effect (see their eqn. 18) which, however, is far too small to explain the observed increase in σ_v.

The final possibility is that the TF scatter decreases significantly with distance, which seems reasonable, since the scatter tends to decrease for high-linewidth galaxies, and these are seen preferentially at large distances. Because of the covariance between σ_v and σ_{TF} (see V1), this could lead to an overestimation of σ_v and an underestimation of σ_{TF}. In this context, it is interesting to note that a power spectrum analysis of the same SFI dataset, like the one performed by Freudling et al. (1999), also returns different results if computed separately for the closer and more distant halves of the sample. However, such analysis reveals that it is the inner part of the sample which has an apparently enhanced σ_v. Given these conflicting results, we consider it unlikely that the apparent increase in σ_v reflects a true property of the velocity field. In any case, it is worth stressing that the increase of σ_v with distance does not affect the estimate of β_I which, as shown in fig. 4 and table 3, does not show significant variations.

9 SUMMARY AND CONCLUSIONS

We have implemented, tested and used the VELMOD technique (V1, V2) to compare the model velocity field obtained from the spatial distribution of PSCz galaxies with the velocities of field spiral galaxies within 6000 km s^{-1} in the SFI catalogue. This comparison allowed us to estimate the value of the β_I parameter, the amplitude of the small-scale velocity noise, σ_v, and to calibrate the TF relation of SFI galaxies.

VELMOD returns an estimate of β_I which is very robust to various systematic and random errors that may enter the analysis at various stages. For the full sample, we obtain $\beta_I = 0.42 \pm 0.04$, while a value of $\beta_I = 0.45 \pm 0.05$ is obtained when a more conservative cut at 4000 km s^{-1} is applied to the SFI sample.

The slope of our TF relation is in good agreement with that obtained from the calibration of the TF relation by G97 using SCI galaxies. However, we find a significantly larger TF scatter ($\sigma_{TF} = 0.44$) than the average scatter found by G97 ($\sigma_{TF} = 0.36$), and a significantly larger zero point ($A_{TF} = -5.89$ *vs* $A_{TF} = -6.09$). We thus conclude that the scatter in the TF relation for field galaxies is larger and the zero point is smaller than the correspoding values for galaxies in clusters, confirming the results of D98 and Freudling *et al.* (1999). Our analysis also confirms that the TF scatter decreases with increasing galaxy rotation velocity, but this does not affect our estimates of β_I. We have also found that the velocity noise, σ_v, increases with distance up to ~ 500 km s^{-1} and is significantly larger than the values obtained by V1 and V2. Although the meaning of such a large σ_v is not clear, it is reassuring that it does not affect the general result of the VELMOD analysis and, in particular, the value of β_I.

In summary, we have found that the PSCz velocity model provides a satisfactory fit to the velocities of SFI galaxies when a value of $\beta_I = 0.42 \pm 0.04$ is used. This value is in good agreement with most of the recent v-v analyses that use the IRAS gravity field, inferred either from the 1.2Jy or the PSCz surveys, irrespective of the type of distance indicator used. Indeed, values of β_I in the range 0.4 - 0.6 are found using the TF relation for spiral galaxies (Davis *et al.* 1996, V1, V2, D98), the $D_n - \sigma$ relation for early type galaxies (Nusser *et al.* 2000), Type Ia Supernovae (Riess *et al.* 1997) and the "surface brightness fluctuations" method in nearby galaxies (Blakeslee *et al.* 2000). Our estimate of β_I is also consistent with the results of v-v analyses which use a model gravity field derived from optical galaxies in the ORS survey (Santiago *et al.* 1995, 1996), once the stronger clustering of optical galaxies is taken into account.

These values of β_I from v-v analyses are significantly smaller than those found using d-d methods (e.g. Sigad *et al.* 1998), even when both are applied to identical datasets. Further support for high values of β comes from power spectrum analyses of various velocity catalogues (Zaroubi *et al.* 1997, Freudling *et al.* 1999, Zaroubi *et al.* 2000), although in this case it is possible that accounting for nonlinear effects may help reduce the discrepancy (Silberman *et al.* 2000). Since v-v methods generally rely on the deviations of a set of observed velocities from a set of model velocities, differences between the two sets do not contribute to β but to the random errors, whereas this is not the case in power spectrum analyses.

A different explanation for the discrepancy between v-v and d-d methods is that the v-v analyses are affected

by non-linear effects. All v-v methods implemented so far assume linear biasing and most of them also use linear gravitational instability theory. Recently new methods have been introduced to measure the nonlinearity in the bias relation in redshift surveys (e.g. Matarrese, Verde & Heavens 1997, Szapudi 1998, Sigad, Branchini & Dekel 2000, Feldman *et al.* 2000) and some of these have been applied to the PSCz survey. For example, Branchini *et al.* (in prep.) have applied the technique of Sigad *et al.* (2000) to the PSCz sample. Their preliminary results indicate that deviations from linear biasing are small and manifest themselves mainly as a anti-bias in low density regions. The amplitude of these effects can only lead to a modest increase of β_I, of the order of $\sim 10\%$. Nonlinear motions might also change the value of β_I. However, Shaya, Peebles & Tully (1995) used a fully nonlinear model of the velocity field and still recovered a low value of β. Similarly, V1 performed a nonlinear VELMOD analysis in an attempt to break the degeneracy between Ω_m and b_I and found indirect evidence that nonlinear motions are already accounted for in the model velocity field when this is predicted from a smooth density field. These results suggest that a treatment of nonlinear effects and the inclusion of nonlinear biasing prescriptions in v-v analyses will not change the inferred value of β significantly. Thus, it seems unlikely that the disagreement between the two methods will be eliminated purely by improving the existing v-v techniques.

ACKNOWLEDGMENTS

It is a pleasure to acknowledge Avishai Dekel, Adi Nusser and Saleem Zaroubi for many useful discussions. A special thanks goes to Michael Strauss for his very useful suggestions and for providing some of the Mark III subsamples used in the original VELMOD analysis. For these same reasons we would have liked to thank Jeff Willick who died in tragic circumstances. EB thanks ESO for its hospitality, where part of this work was done. This work has been partially supported by US NSF grants AST–9528860 to MPH, AST–9617069 to RG and AST–9900695 to RG and MPH and by a UK PPARC rolling grant to CSF. IZ was supported by the DOE and the NASA grant NAG 5-7092 at Fermilab.

REFERENCES

Aaronson M. *et al.* 1982, ApJS, 50, 241
Beichman,C.A., Neugebauer,G., Habing,H.J., Clegg,P.E., Chester,T.J. 1988.
Bertschinger E., Dekel A. 1989, ApJ, 336, L5
Blakeslee J. *et al.* 2000, in Cosmic Flows 1999: Towards an Understanding of Large-Scale Structures, eds. Courteau S., Strauss M., Willick J. (ASP Conference series) p. 254
Bothun G., Mould J. 1987, ApJ, 313, 629
Branchini E. *et al.* 1999, MNRAS, 308, 1 [B99]
Canavezes A. *et al.* 1998, MNRAS, 297, 777
Cole S., Hatton S., Weinberg D., Frenk C. 1998, MNRAS, 300, 945
Courteau S., van den Bergh S. 1999, AJ, 118, 337
da Costa L., Nusser, A., Freudling W., Giovanelli R., Haynes M., Salzer J. Wegner G. 1998, MNRAS, 299, 452 [D98]
da Costa L. *et al.* 2000, AJ, 120, 95
Davis M., Nusser A., Willick J. 1996, ApJ 473, 22
Federspiel M., Sandage A., Tamman G. 1994, ApJ, 430, 29
Feldman H., Frieman J., Fry N., Scoccimarro, R. 2001, PRL, 86, 1434
Fisher K., Huchra J., Strauss M., Davis M., Yahil A., Schlegel D. 1995, ApJS, 100, 69
Freudling W., Martel, H., Haynes M., 1991, ApJ, 317, 1
Freudling W., da Costa L., Wegner G., Giovanelli R., Haynes M., Salzer J. 1995, AJ, 110, 1995
Freudling W, Zehavi, I, da Costa L. N., Dekel A., Eldar A., Giovanelli R., Haynes M. P., Salzer, J. J., Wegner G., Zaroubi S., 1999, ApJ 523, 1
Giovanelli R., Haynes M., Herter T., Vogt N., Wegner G., Salzer J., da Costa L., Freudling W. 1997a, AJ, 113, 22
Giovanelli R., Haynes M., Herter T., Vogt N., da Costa L., Freudling W., Salzer J., Wegner G. 1997b, AJ, 113, 53 [G97]
Haynes, M., Giovanelli R., Salzer J., Wegner, G., Freudling W., da Costa L., Herter T., Vogt N. AJ, 1999a, 117, 1668
Haynes, M., Giovanelli R., Chamaraux P., da Costa L., Freudling W., Salzer J., Wegner, G. AJ, 1999b, 117, 2039

Hudson M. 1994, MNRAS, 266, 475
Kolatt T., Dekel A., Ganon G., Willick J.A., 1996, ApJ, 458, 419
Mathewson D., Ford V., Buchhorn M., 1992, ApJS, 81, 412
Matarrese, S., Verde L., Heavens., 1997, MNRAS, 290, 651
Monaco P., Efstathiou G. 1999 MNRAS 308
Nusser A., Davis M. 1994, ApJ, 421, 1L
Nusser A., da Costa L., Branchini Enzo.,Bernardi M., Alonso M., Wegner Gary., Willmer C., Pellegrini P.2000, MNRAS,, 320, L21
Riess A., Davis M., Baker J., Kirschner R. 1997, 488, L1
Santiago B., Strauss M., Lahav O., Davis M., Dressler A. Huchra J. 1995, ApJ, 446, 457
Santiago B., Strauss M., Lahav O., Davis M., Dressler A., Huchra J. 1996, ApJ, 461, 38
Saunders W. *et al.* 2000, MNRAS, 317, 55
Schmoldt I. *et al.* 1999, MNRAS, 304, 893
Shaya E., Peebles J., Tully B. 1995, ApJ, 454, 1
Sigad Y., Dekel A., Strauss M., Yahil A. 1998, ApJ, 495, 516
Sigad Y., Branchini E., Dekel A. 2000, ApJ, 540, 62
Silberman L., Dekel A., Eldar A., Zehavi I. 2001, [astro-ph/0101361] *in press*
Springel V. 1996, Topology and Luminosity Function of the PSCz Redshift Survey, M.Sc. Thesis, Eberhard-Karls-Univerität Tübingen
Sutherland W. *et al.* 1999, MNRAS, 308.289
Strauss M., Willick J., 1995, Phys Rep., 261, 271
Strauss M., Ostriker J., Cen R. 1998, ApJ, 494, 20
Szapudi I. 1990, MNRAS, 300L, 35 Understanding of Large-Scale Structures, eds. Courteau S., Strauss M., Willick J. (ASP Conference series) p. 242
Willick, J. 1994, ApJS, 92, 1
Willick J., Courteau S., Faber S., Burstein D., Dekel A. ApJ, 1995, 446, 12
Willick J., Courteau S., Faber S., Burstein D., Dekel A. Kolatt T. ApJ, 1996, 457, 333
Willick J., Courteau S., Faber S., Burstein D., Dekel A. Strauss M. ApJS, 1997a, 109, 333
Willick, J., Strauss, M., Dekel, A., Kolatt, T. 1997b, ApJ, 486, 629 [V1]
Willick, J., Strauss, M. 1998, ApJ, 486, 629 [V2]
Willick, J. 2001, in Proceedings of the XXXVth Rencontres de Moriond: Energy Densities in the Universe, *in press* [astro-ph/0003232]
Yahil A., Strauss M.A., Davis M., Huchra J.P., 1991, ApJ, 372, 380
Zaroubi S., Zehavi I., Dekel A., Hoffman Y., Kolatt T. 1997, ApJ, 486, 21
Zaroubi S., Bernardi M., da Costa L.N., Hoffman Y., Alonso V., Wegner G., Willmer C.N.A., Pellegrini P.S. 2001, MNRAS *in press* [astro-ph/0005558]

Table 1. VELMOD analysis of mock catalogues. The top row lists the value of the true parameters. The second row lists the mean value, the error on the mean and, in parenthesis, the typical error in a single realization from VELMOD. Column 1: TF zero point ; column 2: TF slope; column 3: TF dispersion; column 4: 1D velocity dispersion (in $\mathrm{km\,s^{-1}}$); column 5: value of β_I.

A_{TF}	b_{TF}	σ_{TF}	σ_v	β_I
-6.1	7.33	0.36	150	1.0
$-6.096 \pm 0.005(0.02)$	$7.31 \pm 0.04(0.16)$	$0.36 \pm 0.002(0.01)$	$150 \pm 7(33)$	$1.01 \pm 0.009(0.04)$

Table 2. VELMOD analysis of Mark III subcatalogues. The corresponding results of the V1 and V2 analyses are quoted in parenthesis. Column 1: Subcatalogue; column 2: TF zero point; column 3: TF slope; column 4: TF dispersion; column 5: 1D velocity dispersion (in $\mathrm{km\,s^{-1}}$); column 6: β_I value and its 1-σ error

Catalogue	A_{TF}	b_{TF}	σ_{TF}	σ_v	β_I
A82	-5.91 (-5.96)	10.43 (10.36)	0.468 (0.464)	159 (125)	0.50 ± 0.07 (0.49 ± 0.08)
MAT	-5.84 (-5.75)	7.06 (7.12)	0.451 (0.453)	180 (125)	0.42 ± 0.10 (0.50 ± 0.11)
MAT2	-5.83 (-5.80)	6.96 (7.16)	0.433 (0.430)	220 (130)	0.44 ± 0.07 (0.52 ± 0.05)

Table 3. VELMOD analysis of various SFI subsamples. Column 1: redshift range (in $\mathrm{km\,s^{-1}}$) and additional cuts; column 2: number of galaxies column 3: TF zero point; column 4: TF slope; column 5: TF dispersion; column 6: 1D velocity dispersion (in $\mathrm{km\,s^{-1}}$); column 7: β_{min} and its 1-σ error

Sample	$\mathrm{N_{gal.}}$	A_{TF}	b_{TF}	σ_{TF}	σ_v	β_I
$cz_{LG} < 6000$	989	-5.89	7.19	0.439	250	0.42 ± 0.04
$cz_{LG} < 6000,\ \eta > -0.1$	640	-5.89	6.74	0.382	230	0.43 ± 0.04
$cz_{LG} < 6000,\ \eta < -0.1$	349	-5.87	7.04	0.498	248	0.39 ± 0.04
$cz_{LG} < 4000$	493	-5.86	7.32	0.415	216	0.45 ± 0.05
$cz_{LG} < 2000$	158	-5.73	6.67	0.454	206	0.42 ± 0.09
$2000 \leq cz_{LG} < 4000$	335	-5.88	7.41	0.410	196	0.44 ± 0.07
$4000 \leq cz_{LG} < 6000$	496	-5.85	7.54	0.420	535	0.40 ± 0.09